



 Cite this: *RSC Adv.*, 2023, 13, 23745

Six metal–organic architectures from a 5-methoxyisophthalate linker: assembly, structural variety and catalytic features†

 Xiao-Xiang Fan, Hong-Yu Wang, Bo Zhang, Xiu-Qi Kang, Jin-Zhong Gu * and Ji-jun Xue*

A methoxy-functionalized isophthalic acid, 5-methoxy isophthalic acid (H_2mia), was used a versatile linker for assembling six new metal(II) compounds under hydrothermal conditions. The obtained products were $[Cu_2(\mu_2-mia)_2(phen)_2(H_2O)_2] \cdot 2H_2O$ (1), $[Mn(\mu_3-mia)(phen)]_n$ (2), $[Co(\mu_2-mia)(2,2'-bipy)(H_2O)]_n \cdot nH_2O$ (3), $[Co(\mu_3-mia)(\mu_2-4,4'-bipy)]_n \cdot nH_2O$ (4), $[Co(\mu_3-mia)(py)_2]_n$ (5), and $[Cd(\mu_2-mia)(py)(H_2O)_2]_n \cdot nH_2O$ (6), where phen(1,10-phenanthroline), 2,2'-bipy(2,2'-bipyridine), 4,4'-bipy(4,4'-bipyridine) or py(pyridine) were incorporated as auxiliary ligands. The crystal structures of 1–6 range from 0D (1) and 1D (2, 3, 5, 6) CPs to a 2D network (4) with a variety of topological types. The catalytic behavior of 1–6 was studied in the cyanosilylation reaction between trimethylsilyl cyanide and aldehydes, resulting in up to 99% yields of products under optimized conditions. Various reaction parameters as well as catalyst recycling and substrate scope were investigated. This study widens the use of H_2mia as a versatile dicarboxylate linker for assembling a diversity of functional metal–organic architectures with remarkable structural features and catalytic properties.

Received 19th June 2023

Accepted 31st July 2023

DOI: 10.1039/d3ra04111e

rsc.li/rsc-advances

Introduction

Coordination polymers (CPs) are currently the most explored crystalline materials in the fields of inorganic and coordination chemistry. Owing to their almost infinite structural and topological diversity,^{1–4} and plethora of unique properties, these compounds have attracted tremendous attention. The research on CPs opened up potential applications of CPs in gas adsorption and separation,^{5–9} sensing,^{10–13} heterogeneous catalysis,^{14–20} and many other areas.^{21–25}

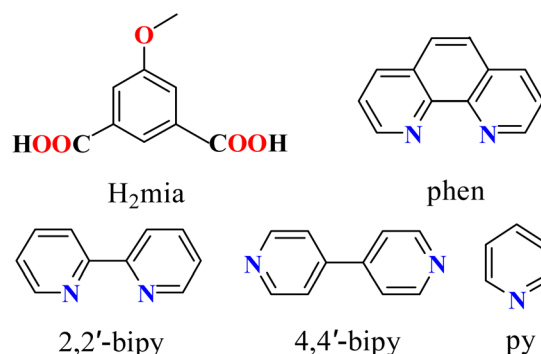
The synthesis of CPs can often be guided for producing definite structural and topological types toward various uses.^{26–30} Despite the significant progress made in this field, structural prediction is not always facile, especially when exploring self-assembly protocols under hydro- or solvothermal conditions. The crystallization of CPs and their final crystal structures might be affected by different factors, including the

type of organic linkers and auxiliary ligands,^{31–33} coordination chemistry of the metal ions involved,^{34,35} type of solvent,^{36,37} reaction temperature^{38,39} and pH.^{40,41}

Aromatic polycarboxylic acids are the most commonly used organic linkers for the synthesis of CPs, because of their adaptable coordination behavior, varying charge and degree of deprotonation, excellent thermal stability, and participation in noncovalent interactions.^{19,20,35,38} Recently, our groups have been focused on designing functional CPs based on multicarboxylate blocks.^{20,42,43} As an extension of this general research direction, herein we selected an underexplored methoxy-functionalized isophthalate ligand, 5-methoxy isophthalic acid (H_2mia , Scheme 1). The organic compound can

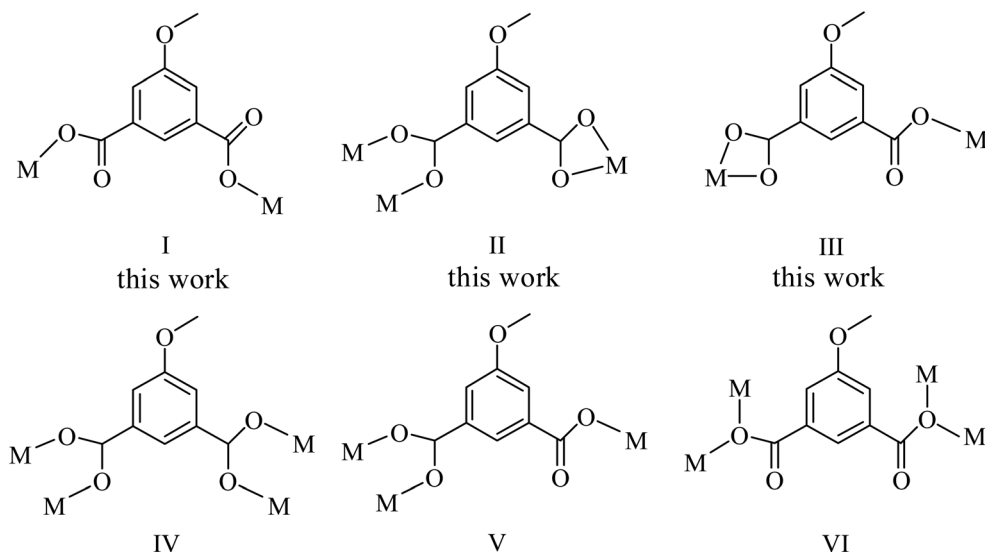
State Key Laboratory of Applied Organic Chemistry, Key Laboratory of Nonferrous Metal Chemistry and Resources Utilization of Gansu Province, College of Chemistry and Chemical Engineering, Lanzhou University, Lanzhou 730000, People's Republic of China. E-mail: gujzh@lzu.edu.cn

† Electronic supplementary information (ESI) available: Analytical data and synthesis for 1–6, FTIR spectra (Fig. S1), PXRD patterns (Fig. S2), temperature dependence of $\chi_M T$ vs. T for compounds 1–5 (Fig. S3), additional catalysis data (Fig. S4–S7) and structural parameters (Tables S1 and S2). The magnetic moments of compounds 1–5 (Table S3), and comparison of catalytic activity (Table S4†). CCDC 2269625–2269630. For ESI and crystallographic data in CIF or other electronic format see DOI: <https://doi.org/10.1039/d3ra04111e>



Scheme 1 Structures of H_2mia and auxiliary ligands.



Scheme 2 Coordination modes of mia^{2-} linkers.

potentially act as a versatile flexible linker for the synthesis of coordination polymers. The selection of the ligand has relied on the following considerations. (1) The H_2mia ligand has a lot of coordination modes and diverse deprotonated types (Scheme 2) according to our survey of the Cambridge Crystallographic Database, which is beneficial for the implementation of unique and interesting networks, such as porous frameworks. (2) The dicarboxylic acid is stable under hydrothermal synthetic conditions. (3) The H_2mia ligand results in diverse structures with excellent luminescent, adsorbing and separating, and magnetic properties.^{44–51} However, only a H_2mia -based network with catalytic properties has been reported.⁵² Thus the present study gave us a good opportunity to develop this field.

This work reports on the hydrothermal synthesis, isolation, characterization, crystal structures, topological features, thermal stability, and catalytic properties of six new coordination compounds prepared from metal(II) chlorides, H_2mia , and various supporting ligands (Scheme 1). The obtained compounds differ from 0D (1) and 1D (2, 3, 5, 6) CPs to a 2D network (4), namely $[\text{Cu}_2(\mu_2\text{-mia})_2(\text{phen})_2(\text{H}_2\text{O})_2] \cdot 2\text{H}_2\text{O}$ (1), $[\text{Mn}(\mu_3\text{-mia})(\text{phen})]_n$ (2), $[\text{Co}(\mu_2\text{-mia})(2,2'\text{-bipy})(\text{H}_2\text{O})]_n \cdot n\text{H}_2\text{O}$ (3), $[\text{Co}(\mu_3\text{-mia})(\mu_2\text{-}4,4'\text{-bipy})]_n \cdot n\text{H}_2\text{O}$ (4), $[\text{Co}(\mu_3\text{-mia})(\text{py})_2]_n$ (5), and $[\text{Cd}(\mu_2\text{-mia})(\text{py})(\text{H}_2\text{O})_2]_n \cdot n\text{H}_2\text{O}$ (6).

Experimental section

General methods

5-Methoxy isophthalic acid (H_2mia) was acquired from Jinan Henghua Sci. & Tec. Co., Ltd. C/H/N analyses were obtained using an Elementar Vario EL elemental analyzer. FTIR spectra (KBr) were recorded on a Bruker EQUINOX 55 spectrometer. TGA measurements were performed on a LINSEIS STA PT1600 thermal analyzer (10 °C min^{-1} heating rate, N_2 flow). PXRD analyses were run on a Rigaku-Dmax 2400 diffractometer (Cu $\text{K}\alpha$ radiation, $\lambda = 1.54060$ Å). Magnetic susceptibility data were collected in the 2–300 K temperature range with a Quantum

Design SQUID Magnetometer MPMS XL-7 with a field of 0.1 T. A correction was made for the diamagnetic contribution prior to data analysis. Solution ^1H NMR spectra were measured on a JNM ECS 400 M spectrometer.

Synthesis of coordination polymers 1–6

The compounds 1–6 were prepared by hydrothermal synthesis, starting from the reaction mixtures composed of copper(II), manganese(II), cobalt(II) or cadmium(II) chlorides, dicarboxylic acid linker, auxiliary ligand, sodium hydroxide, and water as solvent (Table 1). After hydrothermal treatment at 160 °C for three days, the reaction mixtures were gradually (10 °C h^{-1}) cooled to room temperature for crystallization of CPs. Analytical data and detailed synthesis procedures for 1–6 are provided in ESI.†

Crystal structures

Bruker Smart CCD or an Agilent SuperNova diffractometers (Cu $\text{K}\alpha$ radiation, $\lambda = 1.54178$ Å) were used for single-crystal X-ray data collection. SADABS was applied for semiempirical absorption correction. Structure solution by direct methods and refinement by full-matrix least-squares on F^2 was performed on SHELXS-97 and SHELXL-97.⁵³ All atoms (except for hydrogen atoms) were refined anisotropically by full-matrix least-squares methods on F^2 . Hydrogen atoms riding at carbon centers were placed in calculated positions with fixed isotropic thermal parameters and included in final structure factor calculations. Other hydrogen atoms were positioned by difference maps and constrained to ride on their parent O atoms. Some highly disordered solvent molecules in 4 were removed using SQUEEZE routine in PLATON.⁵⁴ The final amount of solvent molecules was estimated from the data of elemental and thermogravimetric analyses. Crystal data are given in Table 2. ESI contains selected bonding and H-bonding parameters (Tables S1 and S2†).



Table 1 Summary of synthetic conditions and assembled products^a

Product formula	Metal(II) precursor	AL ^b	M ²⁺ /linker/AL/NaOH molar ratio	Dimensi-onality
[Cu ₂ (μ ₂ -mia) ₂ (phen) ₂ (H ₂ O) ₂] _n ·2H ₂ O (1)	CuCl ₂ ·2H ₂ O	Phen	1/1/1/2	0D
[Mn(μ ₃ -mia)(phen)] _n (2)	MnCl ₂ ·4H ₂ O	Phen	1/1/1/2	1D
[Co(μ ₂ -mia)(2,2'-bipy)(H ₂ O)] _n ·nH ₂ O (3)	CoCl ₂ ·6H ₂ O	2,2'-Bipy	1/1/1/2	1D
[Co(μ ₃ -mia)(μ ₂ -4,4'-bipy)] _n ·nH ₂ O (4)	CoCl ₂ ·6H ₂ O	4,4'-Bipy	1/1/1/2	2D
[Co(μ ₃ -mia)(py) ₂] _n (5)	CoCl ₂ ·6H ₂ O	py	1/1/31/—	1D
[Cd(μ ₂ -mia)(py)(H ₂ O) ₂] _n ·nH ₂ O _n (6)	CdCl ₂ ·H ₂ O	py	1/1/31/—	1D

^a Hydrothermal synthesis: stainless steel reactor (25 mL volume; Teflon-lined), MCl₂ (0.2 mmol), H₂O (10 mL), 3 days at 160 °C, 10 °C h⁻¹ cooling rate. ^b AL, N-donor auxiliary ligand. The oxidation state of the metals in compounds 1–5 was determined by the values of magnetic moment (Fig. S3 and Table S3).

Table 2 Crystal data for 1–6

Compound	1	2	3	4	5	6
Chemical formula	C ₄₂ H ₃₆ Cu ₂ N ₄ O ₁₄	C ₄₂ H ₂₈ Mn ₂ N ₄ O ₁₀	C ₁₉ H ₁₈ CoN ₂ O ₇	C ₁₉ H ₁₆ CoN ₂ O ₆	C ₁₉ H ₁₆ CoN ₂ O ₅	C ₁₄ H ₁₇ CdNO ₈
Formula weight	947.83	858.56	445.28	427.25	411.27	439.68
Crystal system	Triclinic	Monoclinic	Monoclinic	Triclinic	Monoclinic	Triclinic
Space group	<i>P</i> $\bar{1}$	<i>C</i> 2/ <i>c</i>	<i>P</i> 2 ₁ / <i>c</i>	<i>P</i> $\bar{1}$	<i>C</i> 2/ <i>c</i>	<i>P</i> $\bar{1}$
<i>a</i> /Å	7.3455(7)	38.823(4)	8.8603(3)	10.0273(10)	16.0459(6)	9.3015(5)
<i>b</i> /Å	10.4021(9)	10.4967(8)	17.4505(5)	10.0728(9)	12.0320(4)	10.1706(6)
<i>c</i> /Å	12.8273(10)	18.7612(12)	12.4228(4)	10.7050(14)	19.4535(9)	10.2299(5)
α /°	96.431(7)	90	90	74.711(9)	90	68.453(5)
β /°	92.558(7)	105.531(8)	97.718(3)	66.547(11)	105.900(4)	81.292(4)
γ /°	101.886(8)	90	90	76.120(8)	90	67.661(5)
<i>V</i> /Å ³	950.75(15)	7366.3(11)	1903.37(11)	945.6(2)	3612.1(3)	832.50(9)
<i>T</i> /K	293(2)	293(2)	293(2)	293(2)	293(2)	293(2)
<i>Z</i>	1	8	4	2	8	2
<i>D</i> _c /g cm ⁻³	1.655	1.548	1.554	1.437	1.513	1.754
μ /mm ⁻¹	2.071	6.161	7.480	7.399	7.748	10.901
<i>F</i> (000)	486	3504	916	418	1688	440
Refl. measured	3319	6861	3367	3216	3136	2869
Unique refl. (<i>R</i> _{int})	2810 (0.0239)	3204 (0.0933)	2795 (0.0237)	2712 (0.0329)	2533 (0.0260)	2740 (0.0390)
GOF on <i>F</i> ²	1.065	0.988	1.079	1.017	1.048	1.030
<i>R</i> ₁ [<i>I</i> > 2σ(<i>I</i>)] ^a	0.0434	0.0806	0.0378	0.0536	0.0421	0.0353
w <i>R</i> ₂ [<i>I</i> > 2σ(<i>I</i>)] ^b	0.1153	0.1956	0.0937	0.1351	0.1028	0.0951

^a $R_1 = \sum |F_o| - |F_c| / \sum |F_o|$. ^b $wR_2 = \{\sum [w(F_o^2 - F_c^2)]^2 / \sum [w(F_o^2)]^2\}^{1/2}$.

PXRD patterns for the microcrystalline samples of compounds 1–6 were obtained at room temperature and are given in Fig. S2 (ESI),† along with the diffractograms simulated from CIF files. Both experimental and simulated patterns are in good agreement with what confirms a phase purity of 1–6.

Crystal structures were also analyzed from topological perspective⁵³ by employing the concept of underlying net.^{53,55} Such simplified nets were built by omitting terminal ligands and contracting bridging ligands to centroids, while preserving the connectivity. CCDC-2269625–2269630 contain the supplementary crystallographic data for 1–6.

Catalytic activity in cyanosilylation of benzaldehydes

In a typical procedure for the cyanosilylation of benzaldehydes, a suspension comprising 4-nitrobenzaldehyde (0.50 mmol), trimethylsilyl cyanide (TMSCN, 1.0 mmol), and catalyst (typically 3.0 mol%) in dichloromethane (2.5 mL) was stirred at 35 °C for a desired time. Then, the catalyst was isolated by centrifugation. The obtained solution was evaporated under reduced

pressure, resulting in crude solid. This was dissolved in CDCl₃ and analyzed by ¹H NMR spectroscopy (JNM ECS 400 M spectrometer) for product quantification (further details are given in Fig. S4, ESI†). In the catalyst recycling tests, the catalyst was separated by centrifugation, washed with CH₂Cl₂, dried at 25 °C, and then reused in subsequent runs. Substrate scope using other aldehydes was investigated following the above-described procedure.

Results and discussion

Hydrothermal preparation of 1–6

To explore 5-methoxy isophthalic acid (H₂mia) as a linker in the design of coordination polymers incorporating metal(II) centers (Cu, Mn, Co, or Cd), we performed a number of hydrothermal reactions between the corresponding metal(II) chlorides, H₂mia, NaOH, and auxiliary ligands selected from phen, 2,2'-bipy, 4,4'-bipy, or py. The reactions were carried out for 3 days at 160 °C, followed by crystallization of CPs through a slow cooling of the



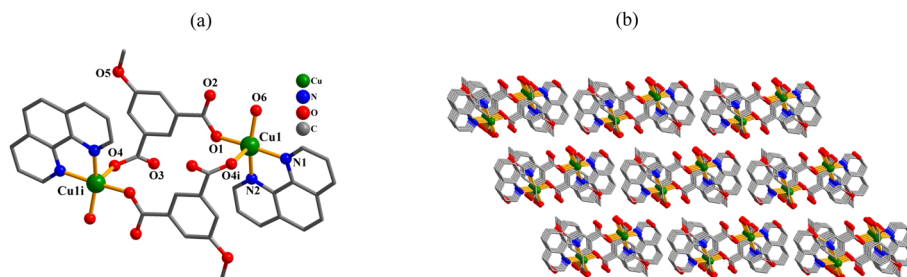


Fig. 1 Structural fragments of **1**. (a) Coordination environment around Cu(II) centers; H atoms are omitted. Symmetry code: (i) = $-x + 2, -y + 2, -z + 2$. (b) 2D supramolecular network; view along the a axis.

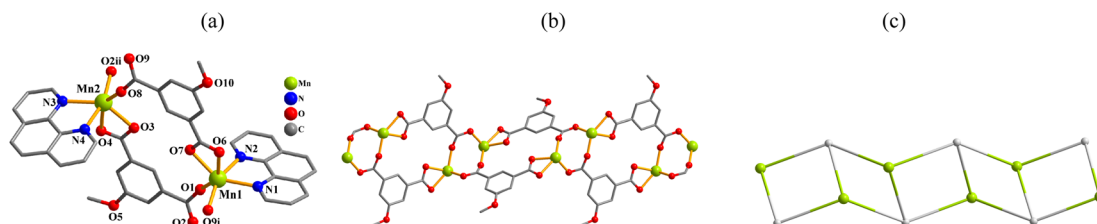


Fig. 2 Structural fragments of **2**. (a) Coordination environment around Mn(II) atoms; H atoms are omitted. Symmetry codes: (i) = $x, -y + 2, z - 1/2$; (ii) = $x, -y + 2, z + 1/2$. (b) 1D metal-organic network; view along the b axis. (c) Topological representation of a mononodal 3-connected ladder chain with a (4,4)(0,2) topology; view along the b axis; 3-linked Mn centers (yellow), centroids of 3-linked μ_2 - mia^{2-} linkers (gray).

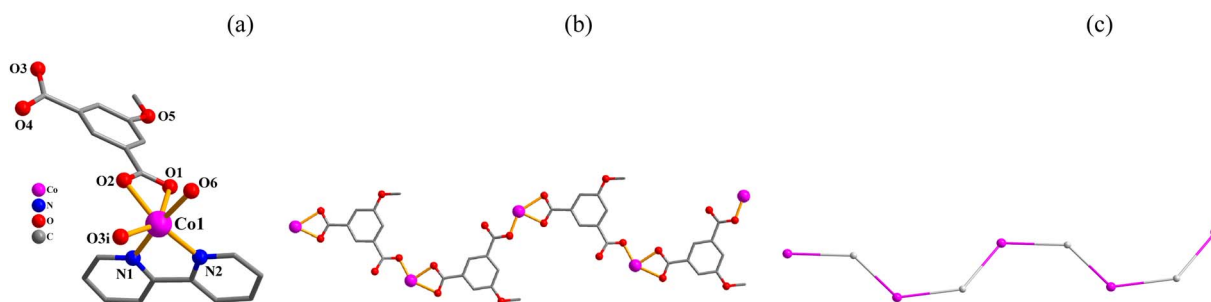


Fig. 3 Structural fragments of **3**. (a) Coordination environment around Co(II) center; H atoms are omitted. Symmetry code: (i) = $-x, y - 1/2, -z + 3/2$. (b) 1D metal-organic chain; view along the a axis. (c) Topological representation of a mononodal 2-linked chain with a 2C1 topology; 2-connected Co1 nodes (pink), centroids of 2-connected μ_2 - mia^{2-} nodes (gray); view along the a axis.

reaction mixtures. Several reaction attempts led to positive results, permitting the generation and full characterization of six new coordination compounds (Tables 1 and 2). These were isolated in good yields as microcrystalline solids, and characterized by C/H/N analysis, FTIR, TGA, PXRD, and single-crystal X-ray diffraction. A variety of structure types observed in **1–6** can be ascribed to differences in coordination preferences of metal(II) centers and the presence of different auxiliary ligands that mediate the crystallization process.

Description of structures

[Cu₂(μ_2 - mia)₂(phen)₂(H₂O)₂]·2H₂O (1**).** Compound **1** shows a discrete dinuclear structure with its asymmetric unit contains one Cu(II) atom, one μ_2 - mia^{2-} ligand, one phen moiety, one H₂O ligand and one lattice water molecule. The Cu1 atom is five-coordinate and shows a distorted square pyramidal {CuN₂O₃}

environment that is made of two carboxylate O donors from two μ_2 - mia^{2-} , one O donor from the H₂O ligand, and two N_{phen} atoms (Fig. 1a). In **1**, the mia^{2-} blocks act as μ_2 -linkers (mode I, Scheme 2) with monodentate COO[−] groups. Which connect copper(II) centers into a Cu₂ molecular unit having a Cu...Cu distance of 8.240(3) Å. These discrete Cu₂ units are interconnected by means of O–H...OH-bonds to give a 3D supramolecular network (Fig. 1b and Table S2, ESI[†]).

[Mn(μ_3 - mia)(phen)]_n (2**).** This structure possesses a 1D chain structure (Fig. 2). The asymmetric unit bears two Mn(II) centers (Mn1, Mn2), two μ_3 - mia^{2-} linkers, and a pair of phen moieties. Both Mn atoms are six-coordinate with distorted octahedral {MnN₂O₄} environments (Fig. 2a), which are occupied by four O atoms from three μ_3 - mia^{2-} linkers and two N_{phen} donors. The mia^{2-} ligands behave as μ_3 -linkers (mode II, Scheme 2), with two COO[−] functionalities adopting bidentate or bridging



bidentate modes. The μ_3 -mia²⁻ linkers connect the Mn(II) centers to generate a 1D ladder-like metal-organic chain (Fig. 2b). The 1D ladder-like chains in this structure are defined as a mononodal 3-connected net (Fig. 2c) with a (4,4)(0,2) topology and a point symbol of (4²·6).

[Co(μ_2 -mia)(2,2'-bipy)(H₂O)]_n·*n*H₂O (3). This 1D coordination polymer is composed of one distinct Co(II) center, one μ_2 -mia²⁻ linker, one 2,2'-bipy moiety, one H₂O ligand and one lattice water molecule per asymmetric unit (Fig. 3). The Co1 atom is six-coordinate and shows a distorted octahedral {CoN₂O₄} environment that is made of three carboxylate O donors from two μ_2 -mia²⁻, one O atom from the H₂O ligand, and two N_{2,2'-bipy} atoms (Fig. 3a). The mia²⁻ ligand functions as a μ_2 -linker (mode III, Scheme 2) with its carboxylate groups being monodentate or bidentate. The mia²⁻ blocks link adjacent cobalt(II) atoms into a 1D metal-organic zigzag chain (Fig. 3b). This structure discloses a mononodal 2-connected network with a 2C1 topology (Fig. 3c).

[Co(μ_3 -mia)(μ_2 -4,4'-bipy)]_n·*n*H₂O (4). This structure features a 2D sheet coordination polymer (Fig. 4). An asymmetric unit possesses one Co atom, one μ_3 -mia²⁻ linker, one 4,4'-bipy ligand, and one lattice water molecule (Fig. 4a). Co1 center is 6-coordinate and unveils a distorted octahedral {CoN₂O₄} environment. It is completed by four carboxylate O atoms from three μ_3 -mia²⁻ linkers and two N_{4,4'-bipy} donors from two different 4,4'-bipy moieties (Fig. 4a). The mia²⁻ block acts as a μ_3 -linker (mode II, Scheme 2) with two COO⁻ groups being

bidentate or bridging bidentate. The 4,4'-bipy moieties adopt a bridging coordination mode. Carboxylate groups of the μ_3 -mia²⁻ blocks link neighbouring Co(II) centers to form a dimeric Co₂ subunit with a Co...Co distance of 4.088(3) Å (Fig. 4b). These Co₂ subunits are further connected by the μ_3 -mia²⁻ linkers and μ_2 -4,4'-bipy ligands into a 2D network (Fig. 4c). The 2D network in this structure is built from the 5-linked Co1, 3-linked μ_3 -mia²⁻ nodes and 2-linked μ_2 -4,4'-bipy nodes (Fig. 4d). It can be defined as a 3-nodal net with a new topology and point symbol of (4²·6.8⁶·12)(4²·6)(8).

[Co(μ_3 -mia)(py)₂]_n (5). This structure features a 1D ladder chain coordination polymer (Fig. 5). An asymmetric unit possesses one Co atom, one μ_3 -mia²⁻ linker, and two py ligands. Co1 center is 6-coordinate and shows a distorted octahedral {CoN₂O₄} environment, which is completed by four carboxylate O atoms from three μ_3 -mia²⁻ blocks and two N_{ipy} donors (Fig. 5a). The mia²⁻ ligand acts as a μ_3 -linker (mode II, Scheme 2) with two COO⁻ groups being bidentate or bridging bidentate, giving a 1D ladder chain (Fig. 5b). The 1D ladder-like chain in this structure is defined as a mononodal 3-connected net (Fig. 5c) with a (4,4)(0,2) topology and a point symbol of (4²·6).

[Cd(μ_2 -mia)(py)(H₂O)₂]_n·*n*H₂O (6). This structure also discloses a 1D metal-organic chain (Fig. 6). In the asymmetric unit, there is one Cd(II) atom, a μ_2 -mia²⁻ linker, a py moiety, two H₂O ligands, and one lattice water molecule. The cobalt(II) center is six-coordinate and features a distorted octahedral {CdNO₅} environment, which is built by three carboxylate O

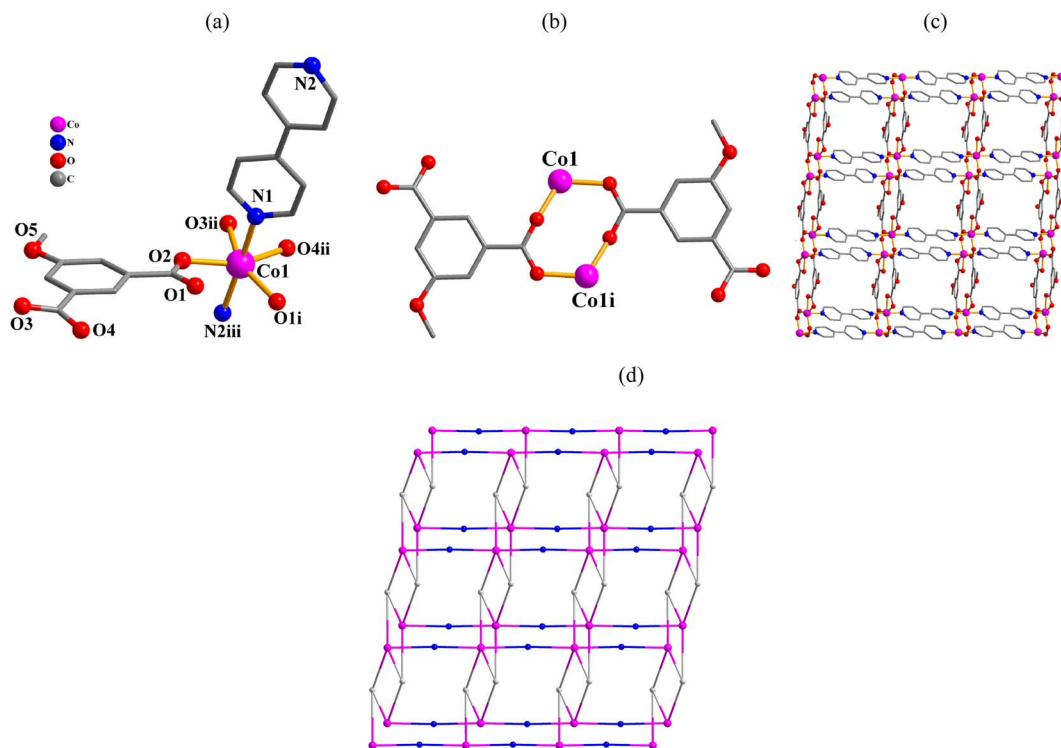


Fig. 4 Structural fragments of 4. (a) Coordination environment around Co(II) center; H atoms are omitted. Symmetry codes: (i) = $-x + 1, -y + 1, -z + 1$; (ii) = $x, y + 1, z$; (iii) = $x - 1, y, z + 1$. (b) Co₂ subunit. Symmetry code: (i) = $-x + 1, -y + 1, -z + 1$. (c) 2D metal-organic network; view along the *c* axis. (d) Topological representation of a3-nodal network with a new topology; 5-connected Co1 nodes (pink), centroids of 3-connected μ_3 -mia²⁻ nodes (gray), centroids of 2-connected μ_2 -4,4'-bipy linkers (blue), view along the *c* axis.



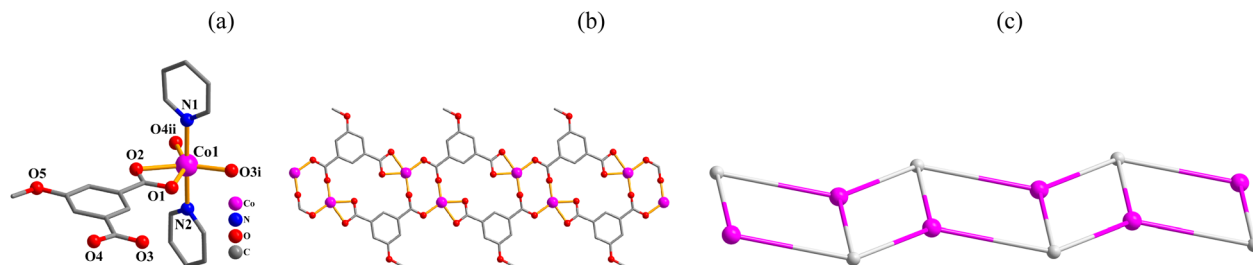


Fig. 5 Structural fragments of **5**. (a) Coordination environment around Co(II) center; H atoms are omitted. Symmetry codes: (i) = $-x + 2, -y + 1, -z + 1$ (ii) = $x + 1/2, y + 1/2, z$. (b) 1D metal-organic ladder chain; view along the *c* axis. (c) Topological representation of a mononodal 3-connected ladder chain with a (4,4)(0,2) topology; view along the *c* axis; 3-connected Co1 nodes (pink), centroids of 3-connected μ_3 -mia²⁻ nodes (gray).

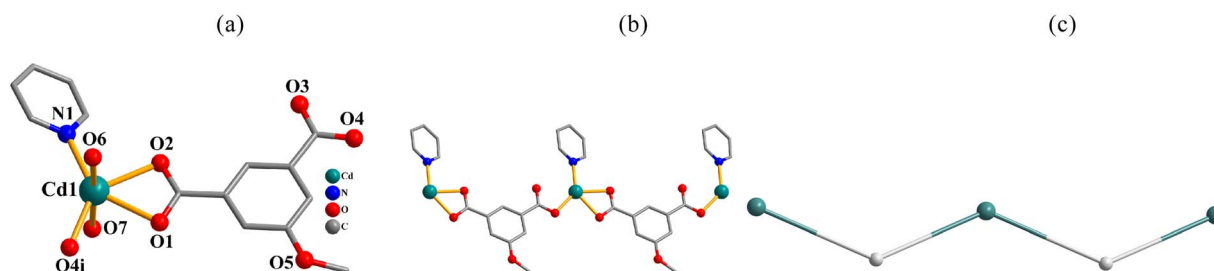


Fig. 6 Structural fragments of **6**. (a) Coordination environment around Cd(II) center; H atoms are omitted. Symmetry code: (i) = $x, y, z - 1$. (b) 1D metal-organic chain; view along the *b* axis. (c) Topological representation of a mononodal 2-connected network with a 2C1 topology; view along the *b* axis; 2-connected Cd1 nodes (turquoise balls), centroids of 2-connected μ_2 -mia²⁻ nodes (gray).

atoms from two μ_2 -mia²⁻ blocks, two O donors from two H₂O ligands, and one N_{py} donor (Fig. 6a). The mia²⁻ block functions as a μ_2 -linker (mode II, Scheme 2), in which one COO⁻ group is monodentate while another group is bidentate. The μ_2 -mia²⁻ blocks connect Cd(II) centers to form a 1D zigzag chain (Fig. 6b). This structure discloses a mononodal 2-connected network with a 2C1 topology (Fig. 6c).

Structural comparison of 1–6

In the obtained compounds **1–6**, 5-methoxy isophthalic acid (H₂mia) act as mia²⁻ ligand showing three distinct coordination fashions, respectively (Scheme 2). Complexes **1** and **2** were synthesized under the same reaction conditions, except for metal chlorides (CuCl₂·2H₂O for **1** and MnCl₂·4H₂O for **2**). Their structural differences unambiguously indicate that the assembly process is metal ion-dependent. The structural change between **3** and **4** caused by adding different auxiliary ligands (2,2'-bipy in **3** and 4,4'-bipy in **4**) under the same reaction conditions. These results imply that the reaction conditions including metal ions and auxiliary ligands have significant effects on the formation and structures of the resulting complexes. Despite similarity of synthesis conditions (Table 1), the obtained compounds show distinct compositions, dimensionalities, and topologies.

Thermal stability

Thermogravimetric analysis (TGA) for **1–6** was carried out under N₂ atmosphere with a heating rate of 10 °C min⁻¹ (Fig. 7). For **1**,

there is a loss of two crystallization water molecules and two H₂O ligands in the 62–194 °C range (exptl, 7.3%; calcd, 7.6%), followed by a decomposition above 240 °C. CP **2** does not contain crystallization solvent or temperature-sensitive ligands, maintaining stability up to 398 °C. For **3**, a release of one lattice water molecule and one water ligand is observed in the 108–158 °C range (exptl, 7.8%; calcd, 8.1%); the remaining solid maintains stability until 217 °C. For **4**, a loss of crystallization H₂O molecule is seen in the 65–157 °C interval (exptl, 4.0%; calcd, 4.2%); the metal-organic network is stable up to 358 °C. The TGA curve of **5** shows a release of two py ligands between

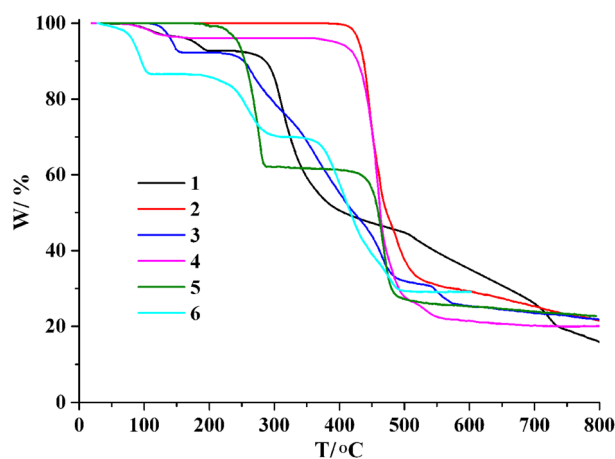
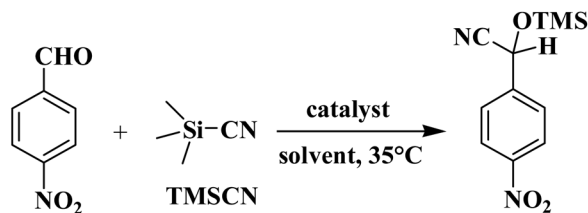


Fig. 7 TGA plots of **1–6** (10 °C min⁻¹, 25–800 °C, N₂ atmosphere).





Scheme 3 Cyanosilylation of model substrate (4-nitrobenzaldehyde).

Table 3 Cyanosilylation of 4-nitrobenzaldehyde with TMSCN^a

Entry	Catalyst	Reaction time, h	Catalyst loading, mol%	Solvent	Product yield ^b (%)
1	1	1	3.0	CH ₂ Cl ₂	37
2	1	2	3.0	CH ₂ Cl ₂	68
3	1	4	3.0	CH ₂ Cl ₂	80
4	1	6	3.0	CH ₂ Cl ₂	89
5	1	8	3.0	CH ₂ Cl ₂	96
6	1	10	3.0	CH ₂ Cl ₂	>99
7	1	10	2.0	CH ₂ Cl ₂	95
8	1	10	3.0	CH ₃ CN	88
9	1	10	3.0	THF	85
10	1	10	3.0	CH ₃ OH	97
11	1	10	3.0	CHCl ₃	95
12	2	10	3.0	CH ₂ Cl ₂	86
13	3	10	3.0	CH ₂ Cl ₂	90
14	4	10	3.0	CH ₂ Cl ₂	81
15	5	10	3.0	CH ₂ Cl ₂	84
16	6	10	3.0	CH ₂ Cl ₂	80
17	Blank	10	—	CH ₂ Cl ₂	5
18	CuCl ₂ ·2H ₂ O	10	3.0	CH ₂ Cl ₂	9
19	H ₂ mia	10	3.0	CH ₂ Cl ₂	6

^a Conditions: 4-nitrobenzaldehyde (0.5 mmol), TMSCN (1.0 mmol), catalyst (2–3 mol%), solvent (2.5 mL), 35 °C. ^b Yield based on ¹H NMR analysis: [moles of product per mol of aldehyde substrate] × 100%.

184 and 288 °C (exptl, 38.2%; calcd, 38.5%), followed by a decomposition above 363 °C. For **6**, there is a loss of one crystallization water molecule, two H₂O ligands and one py ligand in the 32–311 °C range (exptl, 30.0%; calcd, 30.3%), followed by a decomposition above 337 °C.

Catalytic studies

Considering an ability of some coordination polymers to catalyze the cyanosilylation of aldehydes with TMSCN,^{56–59} we tested the obtained products **1–6** as heterogeneous catalysts in this reaction. 4-Nitrobenzaldehyde and TMSCN were used as model substrates for initial screening. The reactions were carried out in CH₂Cl₂ medium at 35 °C to generate 2-(4-nitrophenyl)-2-[(trimethylsilyl)oxy]acetonitrile (Scheme 3 and Table 3). The effects of various reaction parameters were investigated, including the reaction time, type of solvent, catalyst loading and recycling, and substrate scope.

As compound **1** disclosed the highest activity with a quantitative conversion of 4-nitrobenzaldehyde to 2-(4-nitrophenyl)-2-[(trimethylsilyl)oxy]acetonitrile (Table 3), it was selected as

a preferable catalyst in further optimization studies. In particular, the reaction time has a significant effect, as attested by the product yield growth from 37 to >99% on extending the reaction from 1 to 10 h (Table 3, entries 1–6 and Fig. S5, ESI[†]). Catalyst amount was studied, disclosing a slight improvement in the yield from 95 to >99% when changing the catalyst loading from 2 to 3 mol% (entries 6 and 7). Besides acetonitrile, methanol, tetrahydrofuran, and chloroform were screened as solvents but revealed inferior suitability (85–97% product yields).

It is important to indicate that the cyanosilylation of 4-nitrobenzaldehyde is much less efficient in the absence of catalyst (only 5% product yield) or when using H₂mia (6% yield), CuCl₂·2H₂O (9% yield, entries 17–19, Table 3). Despite there is no clear relation between catalyst structure and activity, a slightly superior activity of **1** can be associated with its coordinative unsaturation and better accessibility of active sites.^{20,60,61}

After the above optimization of reaction conditions (3.0 mol% **1**, CH₂Cl₂, 10 h), different substituted benzaldehydes were screened for investigating the substrate scope in the cyanosilylation reaction with TMSCN. The corresponding products were obtained in the yields ranging from 27 to >99% (Table 4). Benzaldehydes with a strong electron-withdrawing substituent (*e.g.*, –NO₂ or –Cl) disclosed the best efficacy (entries 2–5, Table 4), which can be regarded to increased electrophilicity of these substrates. The use of benzaldehydes with an electron-donating group (*e.g.*, –CH₃ or –OCH₃) resulted in inferior product yields (entries 7 and 8, Table 4).

Finally, the recycling of catalyst **1** was attempted. The obtained results (Fig. S6 and S7, ESI[†]) indicate that the compound **1** preserves its activity for at least five reaction cycles, as evidenced by similar product yields. Furthermore, the PXRD patterns confirm that the structure of **1** is retained, despite the observation of several novel signals or widening of some parent peaks. These alterations are common for a recycled catalyst, and can be associated with a decrease in crystallinity and presence of impurities.

The achieved catalytic performance of compound **1** in the cyanosilylation of 4-nitrobenzaldehyde with TMSCN is comparable^{62,63} or superior^{64–69} to those exhibited by the other

Table 4 Substrate scope for Cu-catalyzed cyanosilylation of substituted benzaldehydes with TMSCN^a

Entry	Substituted benzaldehyde (R-C ₆ H ₄ CHO)	Product yield ^b (%)
1	R = H	96
2	R = 2-NO ₂	98
3	R = 3-NO ₂	>99
4	R = 4-NO ₂	>99
5	R = 4-Cl	94
6	R = 4-OH	61
7	R = 4-CH ₃	56
8	R = 4-OCH ₃	27

^a Conditions: aldehyde (0.5 mmol), TMSCN (1.0 mmol), catalyst **1** (3.0 mol%), CH₂Cl₂ (2.5 mL), 35 °C. ^b Yield on the basis of ¹H NMR analysis: [moles of product per mol of aldehyde substrate] × 100%.



heterogeneous catalysts based on other metal–carboxylate coordination compounds (Table S4†).

Conclusions

In summary, six new Cu(II), Mn(II), Co(II), and Cd(II) coordination compounds were generated by facile hydrothermal synthesis and completely characterized. Catalytic properties of the generated products were screened in the cyanosilylation of 4-nitrobenzaldehyde with TMSCN, resulting in close to quantitative yields of product yields, good substrate scope, and possibility of catalyst recycling.

Author contributions

X. X. Fan, J. Z. Gu and J. J. Xue designed the project. H. Y. Wang, B. Zhang and X. Q. Kang performed the synthesis and related measurements. J. Z. Gu carried out the structural characterization. X. X. Fan, J. Z. Gu and J. J. Xue prepared the manuscript. All authors participated in the discussion of experimental results.

Conflicts of interest

There are no conflicts to declare.

Acknowledgements

This work was supported by the 111 Project of MOE (111-2-17).

References

- 1 K. Wang, Y. Li, L.-H. Xie, X. Li and J.-R. Li, *Chem. Soc. Rev.*, 2022, **51**, 6417–6441.
- 2 J. Chen, R. Abazari, K. A. Adegoke, N. W. Maxakato, O. S. Bello, M. Tahir, S. Tasleem, S. Sanati, A. M. Kirillov and Y. Zhou, *Coord. Chem. Rev.*, 2022, **469**, 214664.
- 3 G. Maurin, C. Serre, A. Cooper and G. Férey, *Chem. Soc. Rev.*, 2017, **46**, 3104–3107.
- 4 Y. Bai, Y. Dou, L.-H. Xie, W. Rutledge, J.-R. Li and H.-C. Zhou, *Chem. Soc. Rev.*, 2016, **45**, 2327–2367.
- 5 W. Fan, S. Yuan, W. Wang, L. Feng, X. Liu, X. Zhang, X. Wang, Z. Kang, F. Dai, D. Yuan, D. Sun and H.-C. Zhou, *J. Am. Chem. Soc.*, 2020, **142**, 8728–8737.
- 6 R. Vismara, G. Tuci, N. Mosca, K. V. Domasevitch, C. Di Nicola, C. Pettinari, G. Giambastiani, S. Galli and A. Rossin, *Inorg. Chem. Front.*, 2019, **6**, 533–545.
- 7 W. Fan, X. Wang, X. Liu, B. Xu, X. Zhang, W. Wang, X. Wang, Y. Wang, F. Dai, D. Yuan and D. Sun, *ACS Sustainable Chem. Eng.*, 2019, **7**, 2134–2140.
- 8 X. Zhao, Y. Wang, D. S. Li, X. Bu and P. Feng, *Adv. Mater.*, 2018, **30**, 1705189.
- 9 B. Zheng, X. Luo, Z. Wang, S. Zhang, R. Yun, L. Huang, W. Zeng and W. Liu, *Inorg. Chem. Front.*, 2018, **5**, 2355–2363.
- 10 N. Patel, P. Shukla, P. Lama, S. Das and T. K. Pal, *Cryst. Growth Des.*, 2022, **22**, 3518–3564.
- 11 J. Li, J. F. Tian, H. H. Yu, M. Y. Fan, X. Li, F. B. Liu, J. Sun and Z. M. Su, *Cryst. Growth Des.*, 2022, **22**, 2954–2963.
- 12 A. M. Alsharabasy, A. Pandit and P. Farras, *Adv. Mater.*, 2021, **33**, 2003883.
- 13 Y. Cui, Y. Yue, G. D. Qian and B. L. Chen, *Chem. Rev.*, 2012, **112**, 1126–1162.
- 14 T. Zhang, Z. Zhang, H. Chen, X. Zhang and Q. Li, *Cryst. Growth Des.*, 2022, **22**, 304–312.
- 15 L. Zhao, Z. Du, G. Ji, Y. Wang, W. Cai, C. He and C. Duan, *Inorg. Chem.*, 2022, **61**, 7256–7265.
- 16 K. Li, Y.-F. Liu, X.-L. Lin and G.-P. Yang, *Inorg. Chem.*, 2022, **61**, 6934–6942.
- 17 X. Ma, F. Liu, Y. Helian, C. Li, Z. Wu, H. Li, H. Chu, Y. Wang, Y. Wang, W. Lu, M. Guo, M. Yu and S. Zhou, *Energy Convers. Manage.*, 2021, **229**, 113760.
- 18 Y.-S. Wei, M. Zhang, R. Zou and Q. Xu, *Chem. Rev.*, 2020, **120**, 12089–12174.
- 19 J. Z. Gu, M. Wen, Y. Cai, Z. F. Shi, A. S. Arol, M. V. Kirillova and A. M. Kirillov, *Inorg. Chem.*, 2019, **58**, 2403–2412.
- 20 S. Q. Zhao and J. Z. Gu, *Chin. J. Inorg. Chem.*, 2022, **38**, 161–170.
- 21 Y. Zhu, N. Xin, Z. Qiao, S. Chen, L. Zeng, Y. Zhang, D. Wei, J. Sun and H. Fan, *Adv. Healthcare Mater.*, 2020, **9**, 2000205.
- 22 T. Simon-Yarza, A. Mielcarek, P. Couvreur and C. Serre, *Adv. Mater.*, 2018, **30**, 1705189.
- 23 J. Feng, W.-X. Ren, F. Kong and Y.-B. Dong, *Inorg. Chem. Front.*, 2021, **8**, 848–879.
- 24 Y.-B. Lu, J. Huang, X.-R. Yuan, S.-J. Liu, R. Li, H. Liu, M.-P. Liu, H.-R. Wen, S.-D. Zhu and Y.-R. Xie, *Cryst. Growth Des.*, 2022, **22**, 1045–1053.
- 25 T. Neumann, M. Ceglarska, L. S. Germann, M. Rams, R. E. Dinnebier, S. Suckert, I. Jess and C. Naether, *Inorg. Chem.*, 2018, **57**, 3305–3314.
- 26 W.-H. Huang, X.-X. Zhang and Y.-N. Zhao, *Dalton Trans.*, 2021, **50**, 15–28.
- 27 C. P. Raptopoulou, *Materials*, 2021, **14**, 310.
- 28 X.-D. Zheng and T.-B. Lu, *CrystEngComm*, 2010, **12**, 324–336.
- 29 Q. Guan, L.-L. Zhou and Y.-B. Dong, *Chem. Soc. Rev.*, 2022, **51**, 6307–6416.
- 30 M. P. Merkel, C. E. Anson, G. E. Kostakis and A. K. Powell, *Cryst. Growth Des.*, 2021, **21**, 3179–3190.
- 31 G. Zhan, W. Zhong, Z. Wei, Z. Liu and X. Liu, *Dalton Trans.*, 2017, **46**, 8286–8297.
- 32 G. Fan, L. Hong, X. Zheng, J. Zhou, J. Zhan, Z. Chen and S. Liu, *RSC Adv.*, 2018, **8**, 35314–35326.
- 33 Z. Lei, L. Hu, Z.-H. Yu, Q.-Y. Yao, X. Chen, H. Li, R.-M. Liu, C.-P. Li and X.-D. Zhu, *Inorg. Chem. Front.*, 2021, **8**, 1290–1296.
- 34 Y. Yang, C. Lu, H. Wang and X. Liu, *Dalton Trans.*, 2016, **45**, 10289–10296.
- 35 J. Z. Gu, Y. H. Cui, X. X. Liang, J. C. Wu, D. Y. Lv and A. M. Kirillov, *Cryst. Growth Des.*, 2016, **16**, 4658–4670.
- 36 B. Ramezanpour, M. Mirzaei, V. Jodaian, M. N. Shahrak, A. Frontera and E. Molins, *Inorg. Chim. Acta*, 2019, **484**, 264–275.
- 37 N. Wei, M.-Y. Zhang, X.-N. Zhang, G.-M. Li, X.-D. Zhang and Z.-B. Han, *Cryst. Growth Des.*, 2014, **14**, 3002–3009.
- 38 Y. Li, J. Wu, J.-Z. Gu, A. Qiu Wen and A.-S. Feng, *Chin. J. Struct. Chem.*, 2020, **39**, 727–736.



- 39 X. X. Zou, J. Wu, J. Z. Gu, N. Zhao, A. S. Feng and Y. Li, *Chin. J. Inorg. Chem.*, 2019, **35**, 1705–1711.
- 40 J. Z. Gu, Z. Q. Gao and Y. Tang, *Cryst. Growth Des.*, 2012, **12**, 3312–3323.
- 41 D.-C. Zhong, W.-G. Lu and J.-H. Deng, *CrystEngComm*, 2014, **16**, 4633–4640.
- 42 J. Z. Gu, S. M. Wan, W. Dou, M. V. Kirillova and A. M. Kirillov, *Inorg. Chem. Front.*, 2021, **8**, 1229–1242.
- 43 X. Y. Cheng, L. R. Guo, H. Y. Wang, J. Z. Gu, Y. Yang, M. V. Kirillova and A. M. Kirillov, *Inorg. Chem.*, 2022, **61**, 12577–12590.
- 44 K. Wang, Y. Li, L.-H. Xie, X. Li and J.-R. Li, *Chem. Soc. Rev.*, 2022, **51**, 6417–6441.
- 45 L. McCormick, S. Morris, S. Teat, M. McPherson, A. Slawina and R. Morris, *Dalton Trans.*, 2015, **44**, 17686–17695.
- 46 L.-F. Ma, B. Liu, L.-Y. Wang, C.-P. Li and M. Du, *Dalton Trans.*, 2010, **39**, 2301–2308.
- 47 X.-H. Chang, J.-H. Qin, L.-F. Ma and L.-Y. Wang, *J. Solid State Chem.*, 2014, **212**, 121–127.
- 48 O. Qazvini, V.-J. Scott, L. Bondorf, M. Ducamp, M. Hirscher, F.-X. Coudert and S. Telfer, *Chem. Mater.*, 2021, **33**, 8886–8894.
- 49 Z. Zhang, J. Zhou, H.-X. Sun, M. He, W. Li, L. Du, M. Xie and Q.-H. Zhao, *Cryst. Growth Des.*, 2021, **21**, 5086–5099.
- 50 V.-M. Au, K. Nakayashiki, H. Huang, S. Sugimoto, H. Sato and T. Aida, *J. Am. Chem. Soc.*, 2019, **141**, 53–57.
- 51 L.-F. Ma, J.-W. Zhao, M.-L. Han, L.-Y. Wang and M. Du, *Dalton Trans.*, 2012, **41**, 2078–2083.
- 52 J. Lai, Y. Han, H.-M. Li, J. Wang, C.-L. Wang, L. Suo, Y. Sun and K.-L. Wang, *J. Cluster Sci.*, 2020, **31**, 1389–1398.
- 53 (a) V. A. Blatov, *IUCr CompComm Newsletter*, 2006, vol. 7, pp. 4–38; (b) V. A. Blatov, A. P. Shevchenko and D. M. Proserpio, *Cryst. Growth Des.*, 2014, **14**, 3576–3586.
- 54 A. L. Spek, *Acta Crystallogr., Sect. C: Struct. Chem.*, 2015, **71**, 9–18.
- 55 V. A. Blatov, A. P. Shevchenko and D. M. Proserpio, *Cryst. Growth Des.*, 2014, **14**, 3576–3586.
- 56 J.-J. Du, X. Zhang, X.-P. Zhou and D. Li, *Inorg. Chem. Front.*, 2018, **5**, 2772–2776.
- 57 Y.-M. Xi, Z.-Z. Ma, L.-N. Wang, M. Li and Z.-J. Li, *J. Cluster Sci.*, 2019, **30**, 1455–1464.
- 58 L. M. Aguirre-Díaz, M. Iglesias, N. Snejkó, E. Gutiérrez-Puebla and M. Á. Monge, *CrystEngComm*, 2013, **15**, 9562–9571.
- 59 J. Amaro-Gahete, D. Esquivel, J. R. Ruiz, C. Jiménez-Sanchidrián and F. J. Romero-Salguero, *Appl. Catal., A*, 2019, **585**, 117190.
- 60 E. Loukopoulos and G. E. Kostakis, *J. Coord. Chem.*, 2018, **71**, 371–410.
- 61 L.-P. Xue, Z.-H. Li, T. Zhang, J.-J. Cui, Y. Gao and J.-X. Yao, *New J. Chem.*, 2018, **42**, 14203–14209.
- 62 A. Yadav, S. Kumari, P. Yadav, A. Hazra, A. Chakraborty and P. Kanoo, *Dalton Trans.*, 2022, **51**, 15496–15506.
- 63 W. Jiang, J. Yang, Y.-Y. Liu, S.-Y. Song and J.-F. Ma, *Inorg. Chem.*, 2017, **56**, 3036–3043.
- 64 F. Li, R. Ma, Z. Xia, Q. Wei, S. Chen and S. Gao, *J. Solid State Chem.*, 2021, **301**, 122337.
- 65 A. Karmakar, A. Paul, G. Rúbio, M. Silva and A. Pombeiro, *Eur. J. Inorg. Chem.*, 2016, 5557–5567.
- 66 J.-M. Gu, W.-S. Kim and S. Huh, *Dalton Trans.*, 2011, **40**, 10826–10829.
- 67 F.-Z. Jin, C.-C. Zhao, H.-C. Ma, G.-J. Chen and Y.-B. Dong, *Inorg. Chem.*, 2019, **58**, 9253–9259.
- 68 P. Wu, J. Wang, Y. Li, C. He, Z. Xie and C. Duan, *Adv. Funct. Mater.*, 2011, **21**, 2788–2794.
- 69 Y. Cao, Z. Zhu, J. Xu, L. Wang, J. Sun, X. Chen and Y. Fan, *Dalton Trans.*, 2015, **44**, 1942–1947.

